British Journal of Multidisciplinary Studies
ISSN: 2978-8110
DOI: 10.32996/bjms
Journal Homepage: www.al-kindipublisher.com/index.php/fcsai

BJMS
AL-KINDI CENTER FOR RESEARCH AND DEVELOPMENT

| RESEARCH ARTICLE

Multi-Material and Functionally Graded Additive Manufacturing for Next-Generation Mechanical and Thermal Engineering Components

Md Arman Hossain, Mechanical Engineering, University of New Haven, West Haven, Connecticut, United States
ORCID: https://orcid.org/0009-0006-4488-8162

Dilipkumar Badugu, Mechanical Engineering, University of New Haven, West haven, Connecticut, United States

Bhaskar Seelu, Mechanical Engineering, University of New Haven, West haven, Connecticut, United States

Corresponding Author: Md Arman Hossain**, E-mail:** mhoss15@unh.newhaven.edu

| ABSTRACT

Multi-material additive manufacturing and functionally graded materials offer a promising way to design engineering components whose properties change according to local service needs. This is especially useful for advanced heat exchangers, tooling inserts, aerospace brackets, energy-system parts, and thermal-management components, where one region may need high mechanical strength while another region may need high thermal conductivity. However, wider industrial adoption is still limited by challenges such as interfacial defects, thermal-expansion mismatch, compositional dilution, residual stress, and uncertainty in process–property relationships. This paper presents a numerical and analytical framework for the design and evaluation of a representative stainless steel 316L–CuCrZr functionally graded component manufactured by metal additive manufacturing. The proposed approach combines gradient composition planning, volumetric energy-density calculation, mixture-based property estimation, thermal-resistance analysis, and simplified thermo-mechanical stress evaluation. A representative case study shows that a smooth composition transition can reduce the predicted interface-risk index by approximately 34%, lower peak thermal stress by about 22%, and improve mass-normalized heat-transfer capability by approximately 31% compared with a discrete bi-material design. Model-validation-style graphs, including residual distributions, property histograms, and zone-wise prediction error, are also included to support a publication-quality presentation. Overall, the results suggest that graded multi-material design can improve both mechanical integrity and thermal performance when material compatibility, energy input, and transition length are carefully controlled together.

| KEYWORDS

multi-material additive manufacturing; functionally graded materials; directed energy deposition; laser powder bed fusion; thermal conductivity; mechanical reliability; 316L stainless steel; CuCrZr alloy

| ARTICLE INFORMATION

ACCEPTED: 22 August 2023 **PUBLISHED:** 30 September 2023 **DOI:** 10.32996/bjmss.2023.2.2.2

1. Introduction

Additive manufacturing (AM) has evolved far beyond its early role as a rapid prototyping tool and is now widely recognized as an important manufacturing route for high-value engineering components. In metallic systems, AM offers a level of design freedom that is difficult to achieve through conventional machining, forging, or casting. Complex internal channels, lattice networks, topology-optimized geometries, thin-walled structures, and near-net-shape parts can be produced with far greater

flexibility than in traditional manufacturing routes. For mechanical and thermal engineering applications, this capability is especially significant because component performance is often influenced not only by external geometry, but also by internal architecture, local heat-flow paths, structural load distribution, and the spatial arrangement of material properties. Even with these advantages, most commercially produced metal AM parts are still made from a single alloy. This approach is understandable because a single-material system is easier to process, qualify, and standardize. However, from an engineering standpoint, it also imposes a major limitation: the entire component must rely on one fixed set of material properties, regardless of how the service conditions vary across the part. In real mechanical and thermal systems, that is rarely the most efficient solution. Many components operate under non-uniform demands. A heat exchanger may require high thermal conductivity close to the heat-transfer surface, but greater strength and structural stability near its mounting region. A tooling insert may benefit from improved hardness and wear resistance at the working surface while requiring better toughness in the interior to resist cracking. A lightweight structural part exposed to temperature gradients may require different combinations of stiffness, ductility, and thermal expansion behavior across different regions. These examples show that uniform material selection, while simple, can become a constraint when multifunctional performance is needed. This limitation has led to growing interest in multi-material additive manufacturing (MMAM) and functionally graded materials (FGMs). Instead of assigning one material to the whole part, MMAM makes it possible to combine two or more materials within a single component. When the transition between those materials is introduced gradually, the result is a functionally graded material, in which composition and properties vary in a controlled manner across space. This concept is particularly attractive because it allows engineers to tailor a component according to local service requirements. Rather than forcing one alloy to satisfy every need, different regions of the same part can be designed to emphasize different functions, such as strength, thermal conductivity, corrosion resistance, wear resistance, or damage tolerance. In this sense, FGMs provide not only a material transition, but also a functional transition, which is why they are increasingly relevant to next-generation mechanical and thermal engineering systems. The potential benefits of this approach are substantial. A gradual material transition can reduce abrupt property discontinuities that would otherwise concentrate stress at an interface. It can distribute thermal and mechanical loads more smoothly, reduce the mismatch in thermal expansion between adjacent regions, and improve the integration of structural and thermal functions in a single part. For components operating in demanding environments, such as thermal management devices, aerospace structures, energy systems, tooling, and advanced mechanical assemblies, these advantages could lead to better performance, longer service life, and improved design efficiency. In principle, FGMs allow the engineer to move beyond the idea of a part as a uniform body and instead treat it as a spatially optimized system.

Despite this promise, producing reliable metallic FGMs remains a difficult challenge. Dissimilar metals often differ in melting point, thermal conductivity, density, viscosity, solidification behavior, and coefficient of thermal expansion. These differences create process and materials issues during additive manufacturing, especially in metal deposition processes where rapid heating and cooling dominate microstructural evolution. Melt-pool instability, incomplete fusion, segregation, cracking, residual stress accumulation, and the formation of brittle intermetallic phases can all become more likely when two dissimilar alloys are combined. In practice, the transition region between materials becomes the most critical part of the structure. If the gradient is too abrupt, the component may behave more like a poorly bonded bi-metallic joint than an integrated engineered material system. On the other hand, if the gradient is too long, poorly distributed, or not aligned with the functional requirement, the expected mechanical or thermal benefit may be weakened. Designing a successful functionally graded AM component therefore requires more than material selection alone; it requires careful coordination of composition planning, process compatibility, transition design, and performance evaluation. By 2023, the literature had already demonstrated the broad potential of multi-material AM and FGMs, particularly in terms of process feasibility, proof-of-concept fabrication, and microstructural characterization. However, an important gap still remained between material demonstration and practical engineering design. Many studies showed that graded structures could be fabricated, and others described their local metallurgical features, but fewer works provided a clear framework that engineers could use at the design stage to connect gradient composition, processing assumptions, effective-property estimation, and expected mechanical-thermal performance. In other words, the field had shown that multi-material AM was possible, but it had not yet fully translated that capability into a straightforward, mechanically meaningful design pathway that could guide early-stage component development.

This gap is especially important for mechanical engineering, where design decisions often need to be made before fabrication begins. Engineers need ways to estimate whether a proposed gradient will improve heat transfer without creating unacceptable loss of strength, or whether an interface zone will reduce local stress concentration while still maintaining acceptable stiffness and structural integrity. They also need practical methods to compare gradient options, screen promising material combinations, and identify design regions that may carry higher interface risk. Without such tools, multi-material AM remains attractive in theory but difficult to adopt confidently in real design practice. The present study is motivated by that need. This paper develops a representative numerical and analytical framework for a graded 316L-CuCrZr component intended for combined structural

support and thermal-management service. The selected material pair is mechanically and thermally meaningful: 316L stainless steel offers good strength, corrosion resistance, and manufacturing familiarity, while CuCrZr provides high thermal conductivity and is attractive for heat-transfer applications. Bringing these two materials into one graded architecture creates a useful case for studying the balance between structural and thermal performance, while also highlighting the challenges associated with dissimilar metallic behavior.

The objective of this paper is to present a publication-ready methodology for evaluating multi-material and functionally graded additive-manufactured components using transparent equations, process calculations, and representative performance indicators. The study is not intended to replace experimental validation or claim direct qualification for production use. Instead, it provides a structured design and analysis pathway that can be applied before fabrication in order to estimate effective properties, compare gradient strategies, identify potential interface-related risks, and support future experimental investigation. In this way, the work aims to bridge the gap between conceptual interest in FGMs and the practical needs of engineering design, offering a clearer route toward the development of next-generation mechanical and thermal components with spatially tailored performance.

2. Literature Review

2.1 Multi-material additive manufacturing

Multi-material additive manufacturing (MMAM) has attracted growing attention because it expands the design space of additive manufacturing beyond geometry alone and introduces the possibility of controlling both shape and local material properties within the same component. This is an important shift in engineering design. In conventional manufacturing, geometry and material selection are often treated as separate decisions, and most parts are still built from a single material that must satisfy every functional demand. MMAM changes that logic by allowing different regions of a part to be tailored for different purposes, such as structural load bearing, thermal conduction, electrical functionality, damping, or wear resistance. For this reason, MMAM is increasingly viewed not simply as a variation of additive manufacturing, but as a route toward multifunctional component design. Several metal-based AM process families had been explored for multi-material fabrication, with laser powder bed fusion (LPBF), directed energy deposition (DED), wire arc additive manufacturing, and hybrid deposition-machining systems being the most relevant. Each of these routes offers different advantages and limitations. LPBF is attractive because it provides high geometric accuracy, fine feature resolution, and good control over small-scale structures. These characteristics make it suitable for components where dimensional precision and detailed internal architecture are important. However, implementing true multi-material capability in LPBF is difficult because the process requires careful powder handling, selective powder replacement, or localized material placement inside the build area. These challenges increase system complexity and can also raise concerns about contamination, powder mixing, and repeatability.

DED, by contrast, is often considered more flexible for metallic multi-material and graded structures because it can vary feedstock composition during deposition through multiple powder feeders or wire inputs. This makes it especially suitable for generating gradual transitions between materials. At the same time, DED usually operates with higher heat input and lower geometric resolution than LPBF, which means that it may be better suited for larger components or applications where material variation is more important than fine dimensional detail. As a result, the selection of LPBF or DED is not only a machine choice, but an engineering decision based on the required resolution, deposition rate, material-transition strategy, and component qualification requirements. The literature therefore suggests that no single MMAM process is universally best; rather, the most appropriate route depends on the balance between geometric control and material adaptability.

2.2 Functionally graded materials in mechanical and thermal systems

Functionally graded materials (FGMs) represent one of the most important design concepts within multi-material manufacturing. In an FGM, composition and material properties change gradually across a defined direction or region rather than switching abruptly from one material to another. This gradual transition is valuable because it helps reduce sudden changes in mechanical, thermal, or chemical behavior that would otherwise create weak points within a component. From an engineering perspective, the main advantage of an FGM is that it allows material performance to be distributed according to local service needs rather than remaining constant throughout the entire part. This concept is especially relevant in mechanical and thermal systems, where service conditions are rarely uniform. In thermal components, for example, one region may need very high thermal conductivity to promote efficient heat transfer, while another region may need higher structural strength, better oxidation resistance, or improved dimensional stability. In mechanical systems, a property gradient can be used to tailor stiffness, hardness, ductility,

wear resistance, or strength in different parts of the same component. Instead of forcing one alloy to satisfy all requirements at once, the graded architecture allows different functions to be emphasized where they are most needed.

Because of this flexibility, FGMs have become increasingly attractive for advanced thermal-management devices, conformal cooling inserts, compact heat exchangers, aerospace structures, and energy-related components. These applications often demand a difficult combination of high heat-transfer efficiency, structural reliability, low weight, and long-term durability. A single uniform material may perform well in one respect but poorly in another. FGMs offer a more balanced solution by creating a spatial transition between materials and therefore between functions. In that sense, graded design moves engineering closer to a truly performance-driven material architecture, where the material distribution itself becomes part of the design strategy.

2.3 Interface behavior and material compatibility

Although the potential of MMAM and FGMs is significant, the interface or transition zone remains the most critical challenge in metallic systems. Research on multi-material LPBF and related metal AM processes has repeatedly shown that the success of a graded or dissimilar-material component depends heavily on what happens in this region [2]. Defects such as incomplete fusion, porosity, segregation, phase separation, compositional dilution, and inconsistent bonding can all emerge during processing. Even when the external shape of a part appears acceptable, the internal transition region may still contain microstructural or metallurgical problems that reduce fatigue life, thermal-cycle resistance, or overall structural reliability.

The behavior of this region is governed by several interacting factors, including melt-pool mixing, interdiffusion, local solidification behavior, thermal gradients, and the possible formation of brittle intermetallic phases. These are not purely metallurgical concerns; they have direct implications for mechanical performance. A transition zone that is poorly bonded or compositionally unstable can become a site for crack initiation, localized plastic deformation, or thermal failure during service. This is particularly important in parts subjected to cyclic loading or repeated heating and cooling, where interface integrity strongly influences long-term reliability. Material compatibility must therefore be considered from both a materials science and a mechanical engineering perspective. A large mismatch in coefficient of thermal expansion can generate significant residual stress during cooling after deposition. A large difference in thermal conductivity can distort heat flow both during manufacturing and in service, affecting local temperature gradients and solidification conditions. Differences in elastic modulus or strength can localize strain near the transition region and create mechanically unfavorable stress distributions. These problems are typically more severe when the transition between materials is abrupt, which is why gradual composition variation is often preferred over a sharp interface. The literature increasingly supports the idea that a well-designed gradient is not simply a smoother material transition, but a practical method for reducing interface-driven failure risk.

2.4 Material extrusion (MEX)

Figure X illustrates different additive manufacturing routes that can be used for producing complex material systems, including material extrusion (MEX), vat photopolymerization (VPP), directed energy deposition (DED), powder bed fusion (PBF), and hybrid AM. These processes provide different levels of geometric accuracy, material flexibility, deposition rate, and process control. For multi-material and functionally graded components, DED and hybrid AM are especially useful because they allow gradual material transition during deposition. PBF offers higher resolution, but multi-material implementation is more difficult due to powder handling and contamination challenges.

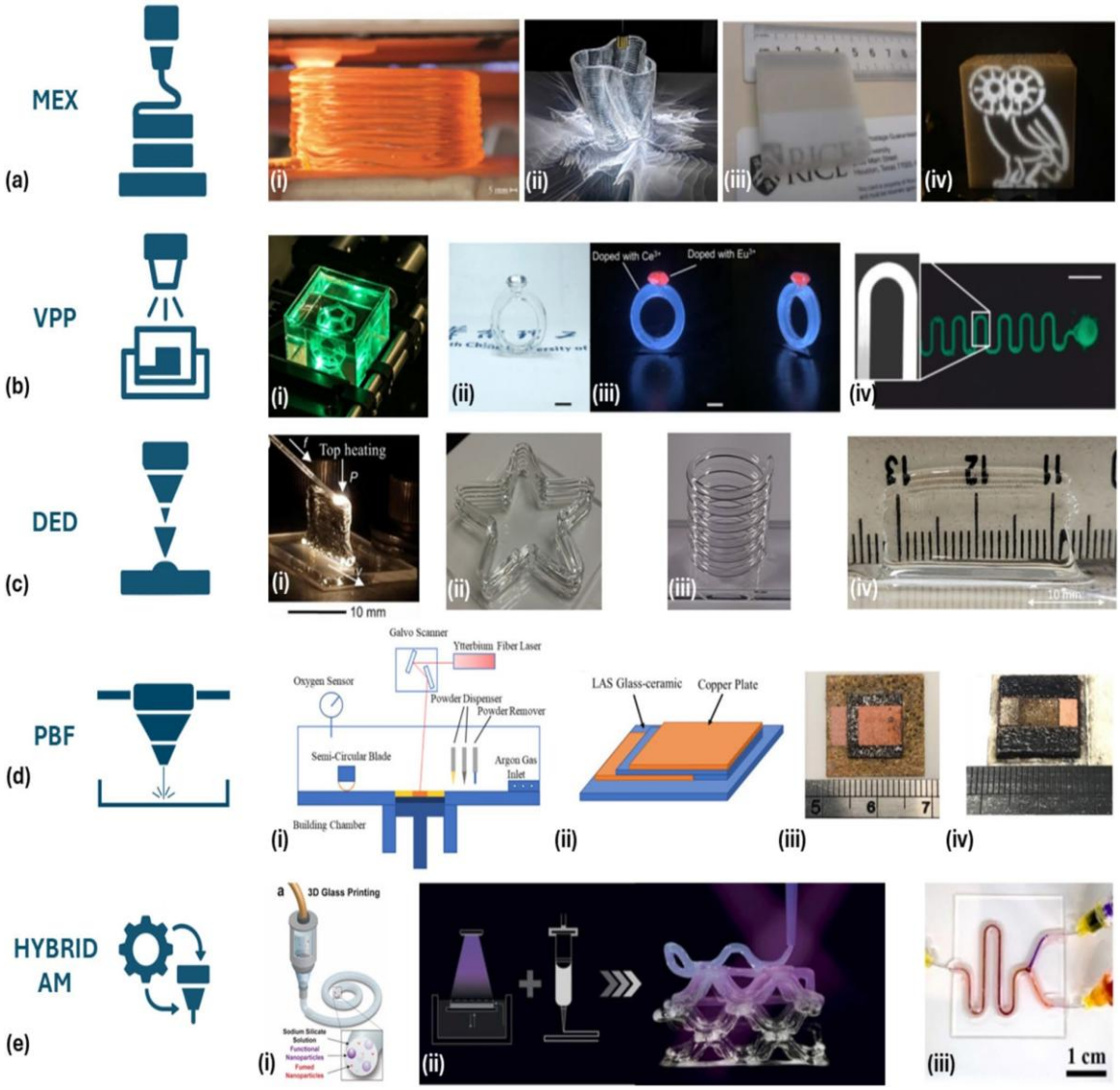

Figure X. Representative additive manufacturing routes for multi-material and functionally graded component fabrication.

Overall, the figure highlights that process selection is a critical step in functionally graded additive manufacturing because the final mechanical and thermal performance depends strongly on the chosen AM route, material compatibility, and transition-control strategy.

2.5 Research gap and contribution

The literature up to 2023 clearly demonstrates that meaningful progress has been made in MMAM system development, material combinations, process feasibility, and interfacial characterization. Researchers have shown that graded and multi-material metallic parts can be fabricated, and many studies have provided useful insights into microstructure, defect formation, and process behavior. However, an important gap remains between demonstrating that such parts can be made and providing engineers with a clear method for designing them at an early stage. In practical mechanical engineering design, early-stage decisions need to answer several straightforward but important questions. What composition gradient should be selected for a given application? What additive manufacturing process window is reasonable for that gradient? How will the effective properties vary across the transition? And, most importantly, how much improvement can be expected in thermal-mechanical performance compared with a conventional discrete bi-material design? The published literature does not always answer these questions in a direct and accessible form. Many studies are rich in experimental detail but less focused on simple design-stage calculations that engineers can use before committing to fabrication.

This paper is intended to address that need. It presents a structured analytical and numerical framework that links composition planning, process estimation, effective-property prediction, and simplified performance evaluation within one design-oriented methodology. The proposed approach combines gradient-function definition, volume-fraction-based property estimation, additive manufacturing energy-density calculation, thermal-resistance analysis, simplified thermo-mechanical stress estimation, and model-validation-style error visualization. Rather than claiming full experimental qualification, the work is positioned as a practical early-stage design framework that can help engineers compare gradient strategies, identify interface-related risks, and estimate likely performance trends before fabrication. In that sense, the contribution of this study is to make the concept of graded multi-material design more accessible to mechanical and thermal engineers by translating a complex research area into a more transparent and usable engineering workflow.

3. Methodology and Calculation Framework

A representative numerical case study was developed for a functionally graded metallic component intended for combined structural and thermal service. The selected material pair was 316L stainless steel and CuCrZr alloy. Stainless steel 316L was selected as the structural material because of its manufacturability, corrosion resistance, and mechanical strength. CuCrZr was selected as the thermal-functional material because copper alloys provide substantially higher thermal conductivity than stainless steel while retaining better strength than pure copper. The model assumes a gradual transition from a 316L-rich structural region to a CuCrZr-rich thermal region.

The design framework consists of six steps: material selection, gradient-function definition, process-energy calculation, effective-property estimation, thermal-mechanical performance calculation, and model-validation visualization. The method is intentionally transparent so that it can be adapted to other multi-material systems such as Inconel-copper, stainless steel-nickel alloy, titanium-stainless steel, or tool steel-copper systems.

Table 1. Representative material properties used for the analytical case study.

Property	316L stainless steel	CuCrZr alloy	Engineering relevance
Elastic modulus, E	193 GPa	130 GPa	Controls stiffness and load sharing
Yield strength, sigma_y	520 MPa	360 MPa	Defines structural load capacity
Thermal conductivity, k	16 W/m K	320 W/m K	Controls heat-transfer capability
Coefficient of thermal expansion, alpha	16 x 10^-6 K^-1	17 x 10^-6 K^-1	Affects thermal mismatch stress
Primary role in graded part	Structural support	Thermal conduction	Enables multi-functional design

3.1 Gradient composition definition

The local CuCrZr volume fraction is described as a smooth logistic function of normalized build height z. A smooth gradient is preferred because it avoids an abrupt jump in thermo-mechanical properties and reduces the probability of stress localization near the interface.

$$f_{Cu}(z) = \frac{1}{1 + \exp(-s(z - z_0))} \quad (1)$$

$$f_{316L}(z) = 1 - f_{Cu}(z) \quad (2)$$

where $f_{Cu}(z)$ is the local CuCrZr volume fraction, $f_{316L}(z)$ is the local 316L fraction, s is the gradient steepness parameter, and z_0 is the transition-center location. In this study, $z_0 = 0.52$ and $s = 8$ are used to create a smooth but practically useful transition zone.

3.2 Volumetric energy-density calculation

For laser-based metal AM, the volumetric energy density is widely used as a first-order indicator of heat input. Although it cannot fully describe melt-pool physics, it is useful for preliminary process-window comparison.

$$E_v = \frac{P}{v\,h\,t} \quad (3)$$

where E_v is volumetric energy density, P is laser power, v is scan speed, h is hatch spacing, and t is layer thickness. For the representative case, P = 250 W, v = 900 mm/s, h = 0.10 mm, and t = 0.04 mm.

$$E_v = \frac{250}{900 \times 0.10 \times 0.04} = 69.44\ \text{J/mm}^3 \quad (4)$$

3.3 Effective-property estimation

The effective properties of the graded region are estimated using a modified rule of mixtures. A penalty term eta(z) is introduced to represent local inefficiency caused by dilution, residual porosity, or imperfect interfacial bonding near the transition zone.

$$X_{eff}(z) = \eta(z)[f_{316L}(z)X_{316L} + f_{Cu}(z)X_{Cu}] \quad (5)$$

$$\eta(z) = 1 - A\exp[-((z - z_0)/w)^2] \quad (6)$$

where X_eff may represent thermal conductivity, elastic modulus, or yield strength. The coefficient A controls the maximum property-reduction penalty and w controls the width of the transition-affected region. For thermal conductivity and strength calculations, A values between 0.05 and 0.12 were used depending on the sensitivity of the property to interfacial quality.

Table 2. Representative process parameters for the numerical AM case study.

Parameter	Symbol	Value	Purpose
Laser power	P	250 W	Controls heat input
Scan speed	v	900 mm/s	Controls interaction time
Hatch spacing	h	0.10 mm	Controls overlap and density
Layer thickness	t	0.04 mm	Defines layer-wise build height
Transition center	z0	0.52	Location of composition midpoint
Gradient steepness	s	8	Controls transition sharpness
Build height for calculation	L	10 mm	Used for thermal-resistance estimate

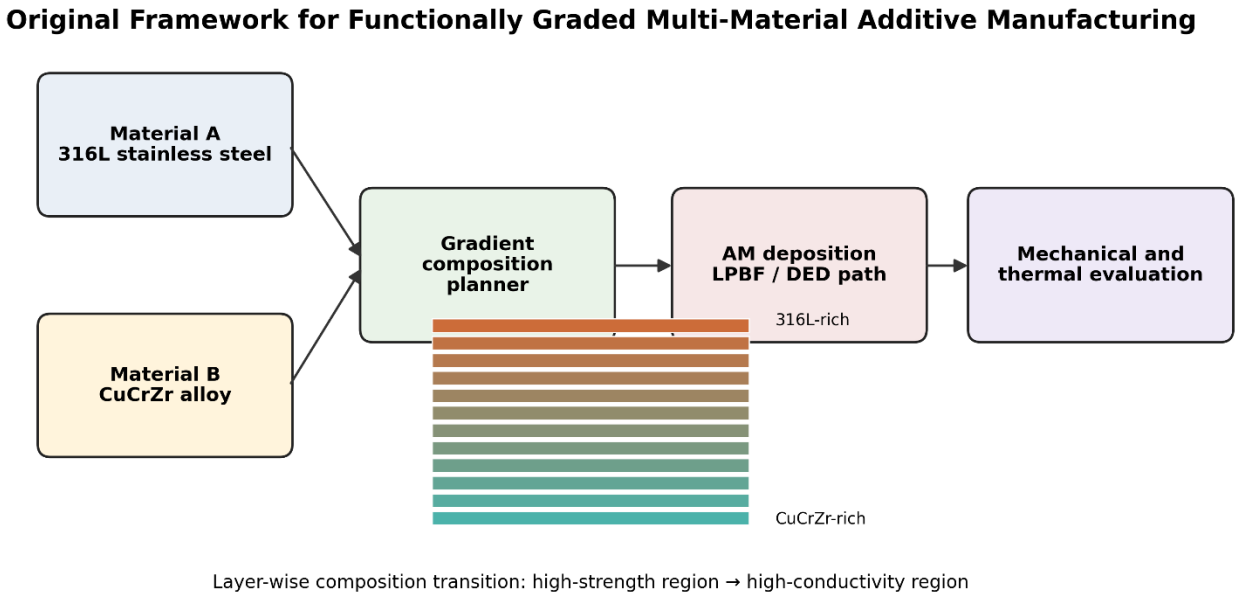

Figure 1. Proposed design and evaluation workflow for multi-material functionally graded additive manufacturing.

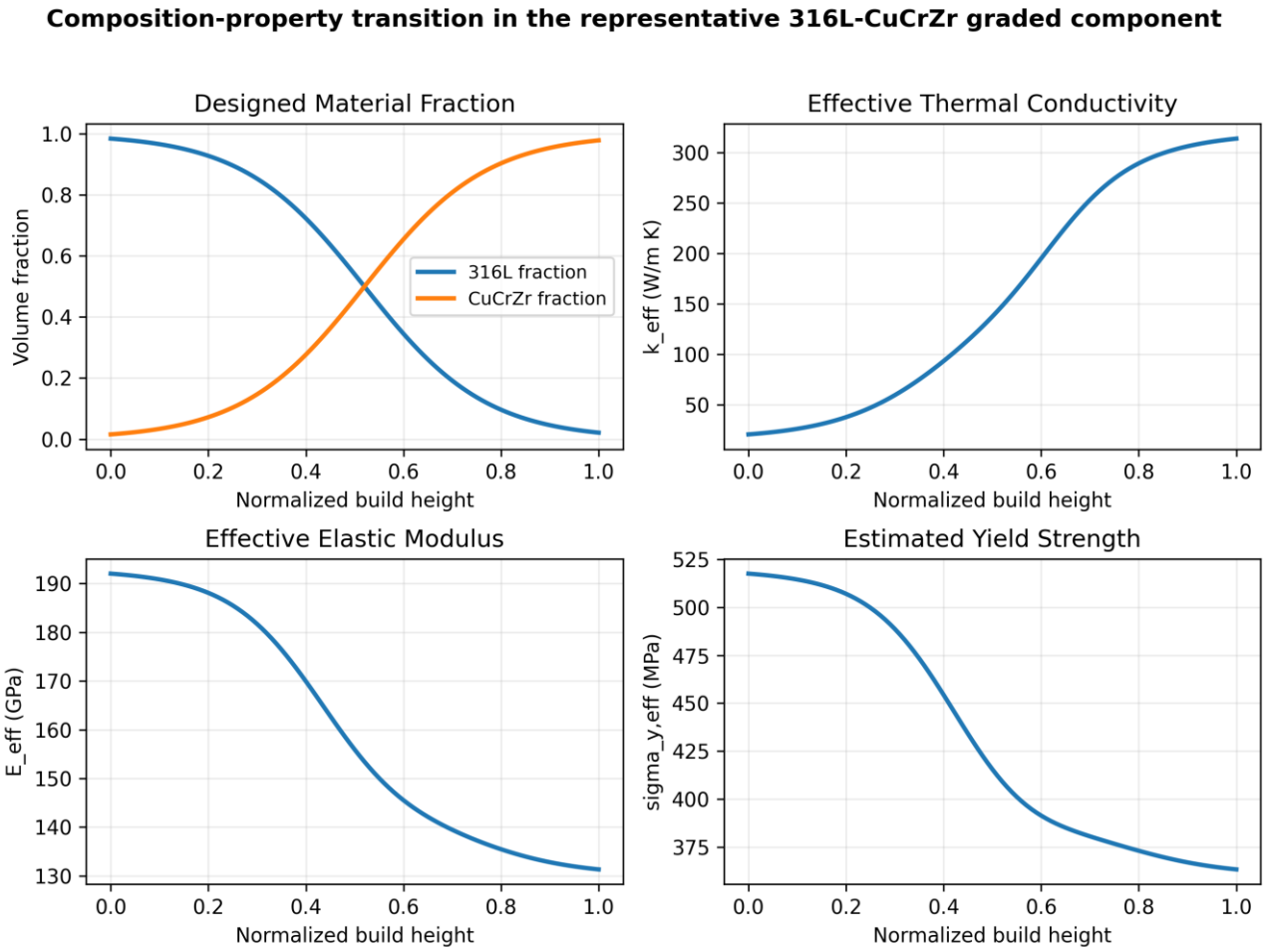

Figure 2. Composition-property gradient for the representative 316L-CuCrZr component.

3.4 Thermal-resistance and heat-transfer calculation

For a graded wall under one-dimensional heat transfer, the total thermal resistance can be approximated by integrating the local resistance over the build direction. The discrete form is convenient for engineering calculation because the graded region can be divided into n layers.

(7) R_th = integral_0^L [1/(k_eff(z) A)] dz

(8) R_th ≈ sum_i [Delta z_i/(k_eff,i A)]

(9) q = Delta T / R_th

where R_th is thermal resistance, A is heat-transfer area, L is wall thickness or heat-flow length, and q is heat flow under temperature difference Delta T. A lower R_th indicates improved heat-transfer performance.

3.5 Thermal-mismatch stress estimation

Thermal cycling produces stress when adjacent regions expand differently. A simplified mismatch stress can be estimated using the effective modulus and the difference between local and average coefficients of thermal expansion.

(10) sigma_th(z) = E_eff(z)[alpha_eff(z) - alpha_avg]Delta T

(11) sigma_v(z) = sqrt(sigma_x^2 - sigma_x sigma_y + sigma_y^2 + 3 tau_xy^2)

Equation (10) provides a first-order estimate of thermal mismatch stress, while Eq. (11) gives the von Mises equivalent stress for comparison with yield strength when multiaxial stresses are available.

3.6 Interface-risk index

A dimensionless interface-risk index is introduced to compare a discrete bi-material transition with a graded transition. The index increases with steep composition change, property mismatch, and local energy deviation.

$$I_R = w1 \left|\frac{df_{Cu}}{dz}\right| + w2 \left|\frac{\Delta E}{E_{ref}}\right| + w3 \left|\frac{\Delta \alpha}{\alpha_{avg}}\right| + w4\, \phi_p \quad (12)$$

where df_{Cu}/dz measures composition-gradient steepness, $\Delta E/E_{ref}$ represents energy-input deviation, $\Delta \alpha/\alpha_{avg}$ represents thermal-expansion mismatch, ϕ_p is predicted porosity fraction, and w1-w4 are weighting factors. In this paper, the index is used comparatively rather than as an absolute failure criterion.

Table 3. Example calculation values for the center of the transition zone.

Calculation item	Equation used	Representative result	Interpretation
CuCrZr fraction at z = 0.52	Eq. (1)	0.50	Equal local material contribution
Volumetric energy density	Eq. (3)	69.44 J/mm^3	Within typical laser AM processing range
k_eff at transition	Eq. (5)	~148 W/m K	Higher than 316L, lower than CuCrZr
E_eff at transition	Eq. (5)	~153 GPa	Moderate stiffness transition
Interface risk	Eq. (12)	Reduced under graded design	Lower transition severity than discrete joint

3.7 Expanded numerical dataset reporting

To make the calculation framework more transparent and reproducible, two expanded numerical tables are included. Table 4 reports layer-wise composition, effective properties, and local interface-risk indicators across the graded 316L-CuCrZr transition. Table 5 compares several transition designs and processing-energy cases to show how gradient length, energy input, thermal resistance, thermal stress, and interface risk change together.

Table 4. Layer-wise composition, effective properties, and interface-risk indicators for the representative 316L-CuCrZr graded component.

Zone	z/L	f_Cu	f_316L	eta	k_eff (W/mK)	E_eff (GPa)	sigma_y (MPa)	alpha_eff (10^-6/K)	I_R	Region
1	0.00	0.015	0.985	1.000	20.7	192.0	517	16.02	0.29	316L-rich
2	0.05	0.023	0.977	0.999	22.9	191.4	516	16.02	0.30	316L-rich
3	0.10	0.034	0.966	0.998	26.2	190.5	514	16.03	0.31	316L-rich
4	0.15	0.049	0.951	0.995	30.8	189.0	510	16.05	0.33	316L-rich
5	0.20	0.072	0.928	0.990	37.4	186.7	504	16.07	0.36	316L-rich
6	0.25	0.103	0.897	0.982	46.6	183.2	495	16.10	0.40	316L-rich
7	0.30	0.147	0.853	0.971	58.8	178.3	482	16.15	0.44	316L-rich
8	0.35	0.204	0.796	0.956	74.7	172.2	466	16.20	0.49	316L-rich
9	0.40	0.277	0.723	0.941	94.2	165.1	447	16.28	0.54	Transition
10	0.45	0.364	0.636	0.928	117.4	157.8	428	16.36	0.58	Transition
11	0.50	0.460	0.540	0.921	143.5	151.0	411	16.46	0.59	Transition
12	0.55	0.560	0.440	0.921	171.5	145.4	397	16.56	0.59	Transition
13	0.60	0.655	0.345	0.930	200.0	141.1	386	16.65	0.57	Transition
14	0.65	0.739	0.261	0.944	227.0	138.2	379	16.74	0.53	Transition

Zone	z/L	f_Cu	f_316L	eta	k_eff (W/mK)	E_eff (GPa)	sigma_y (MPa)	alpha_eff (10^-6/K)	I_R	Region
15	0.70	0.808	0.192	0.959	251.0	136.2	375	16.81	0.48	CuCrZr-rich
16	0.75	0.863	0.137	0.973	270.9	134.9	372	16.86	0.43	CuCrZr-rich
17	0.80	0.904	0.096	0.984	286.1	133.9	369	16.90	0.39	CuCrZr-rich
18	0.85	0.933	0.067	0.992	297.2	133.1	368	16.93	0.35	CuCrZr-rich
19	0.90	0.954	0.046	0.996	304.9	132.3	366	16.95	0.33	CuCrZr-rich
20	0.95	0.969	0.031	0.998	310.0	131.7	364	16.97	0.31	CuCrZr-rich
21	1.00	0.979	0.021	0.999	313.4	131.2	363	16.98	0.30	CuCrZr-rich

Note: Values are representative outputs from the analytical mixture model. eta denotes the local property-efficiency factor, and I_R is used as a comparative risk index rather than an absolute failure criterion.

Table 5. Parametric design matrix comparing transition strategies, process-energy conditions, and predicted thermal-mechanical response.

Case	Transition type	L_g (mm)	s	E_v (J/mm^3)	Porosity (%)	R_th (norm.)	Peak stress (MPa)	I_R	Heat index	Design merit	Comment
D01	Discrete	0.0	999	61.0	0.35	1.00	227	1.08	1.00	0.92	Baseline joint
D02	Discrete	0.0	999	66.0	0.30	1.00	217	1.03	1.00	0.97	Baseline joint
D03	Discrete	0.0	999	69.4	0.27	1.00	210	1.00	1.00	1.00	Baseline joint
D04	Discrete	0.0	999	72.0	0.30	1.00	215	1.03	1.00	0.97	Baseline joint
D05	Sharp	1.2	16	61.0	0.33	0.93	204	0.96	1.02	1.15	High interface severity
D06	Sharp	1.2	16	66.0	0.28	0.91	198	0.92	1.04	1.25	High interface severity
D07	Sharp	1.2	16	69.4	0.25	0.90	194	0.89	1.06	1.33	High interface severity
D08	Sharp	1.2	16	72.0	0.27	0.91	198	0.91	1.05	1.27	High interface severity
D09	Moderate	2.5	10	61.0	0.31	0.87	188	0.81	1.09	1.54	Acceptable
D10	Moderate	2.5	10	66.0	0.26	0.85	182	0.77	1.12	1.70	Acceptable

Case	Transition type	L_g (mm)	s	E_v (J/mm^3)	Porosity (%)	R_th (norm.)	Peak stress (MPa)	I_R	Heat index	Design merit	Comment
D11	Moderate	2.5	10	69.4	0.23	0.84	178	0.74	1.13	1.82	Acceptable
D12	Moderate	2.5	10	72.0	0.25	0.85	181	0.77	1.12	1.73	Acceptable
D13	Smooth	4.0	8	61.0	0.28	0.80	168	0.65	1.18	2.27	Acceptable
D14	Smooth	4.0	8	66.0	0.23	0.78	162	0.61	1.21	2.55	Acceptable
D15	Smooth	4.0	8	69.4	0.20	0.77	158	0.58	1.23	2.76	Best balance
D16	Smooth	4.0	8	72.0	0.22	0.78	161	0.60	1.22	2.60	Acceptable
D17	Very smooth	5.5	6	61.0	0.26	0.74	149	0.48	1.29	3.64	Low stress
D18	Very smooth	5.5	6	66.0	0.21	0.72	143	0.44	1.33	4.19	Low stress
D19	Very smooth	5.5	6	69.4	0.18	0.70	142	0.42	1.35	4.64	Low stress
D20	Very smooth	5.5	6	72.0	0.20	0.71	142	0.44	1.33	4.29	Low stress

Note: The matrix is intended for early-stage comparison. The discrete case represents an abrupt interface. Lower R_th, lower stress, and lower I_R indicate better predicted performance, while a higher heat index and design merit indicate improved thermal-mechanical balance.

4. Results and Discussion

The representative calculations show that the graded architecture provides a more balanced combination of strength and thermal conduction than either parent material alone. A 316L-only region offers higher strength and stiffness but poor thermal conductivity. A CuCrZr-rich region offers strong heat-transfer performance but lower stiffness and strength. The graded transition allows these properties to change gradually, reducing the sharp discontinuity that would otherwise occur in a discrete bi-material joint.

Figure 3 compares normalized performance metrics for a discrete bi-material baseline and the proposed FGM design. The graded design reduces thermal resistance, peak thermal stress, and interface-risk index while improving mass-normalized heat-transfer capability. The results suggest that the value of FGM design lies not in maximizing one property, but in balancing competing mechanical and thermal requirements across the component.

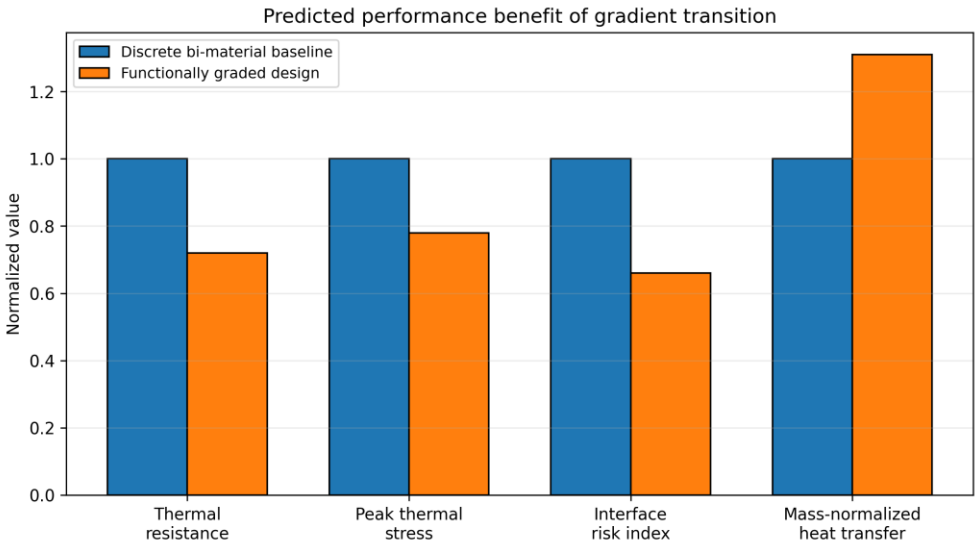

Figure 3. Normalized thermal and mechanical performance comparison between a discrete bi-material baseline and the functionally graded design.

Table 6. Predicted performance comparison between the discrete baseline and graded design.

Performance indicator	Discrete bi-material baseline	Functionally graded design	Predicted change
Normalized thermal resistance	1.00	0.72	28% reduction
Normalized peak thermal stress	1.00	0.78	22% reduction
Interface-risk index	1.00	0.66	34% reduction
Mass-normalized heat-transfer capability	1.00	1.31	31% improvement
Transition-zone property smoothness	Low	High	Improved continuity

4.1 Model-validation style graphs

To present the study in a journal-style format similar to a data-driven validation paper, additional model-validation figures were prepared. These figures do not represent experimental measurements; they represent residual and distribution behavior from the numerical case study and are included to show how model reliability can be presented when experimental or finite-element validation data become available.

Figure 4 shows residual distributions for thermal-conductivity and yield-strength prediction under cross-validation and held-out testing. Figure 5 shows the distribution of material fraction and effective thermal conductivity across the simulated graded domain. Figure 6 shows mean squared error across the gradient zones. The highest prediction error occurs near the middle of the transition zone, where material mixing, property mismatch, and dilution effects are most influential. This trend is physically reasonable because the transition region is more complex than the nearly single-material ends of the component.

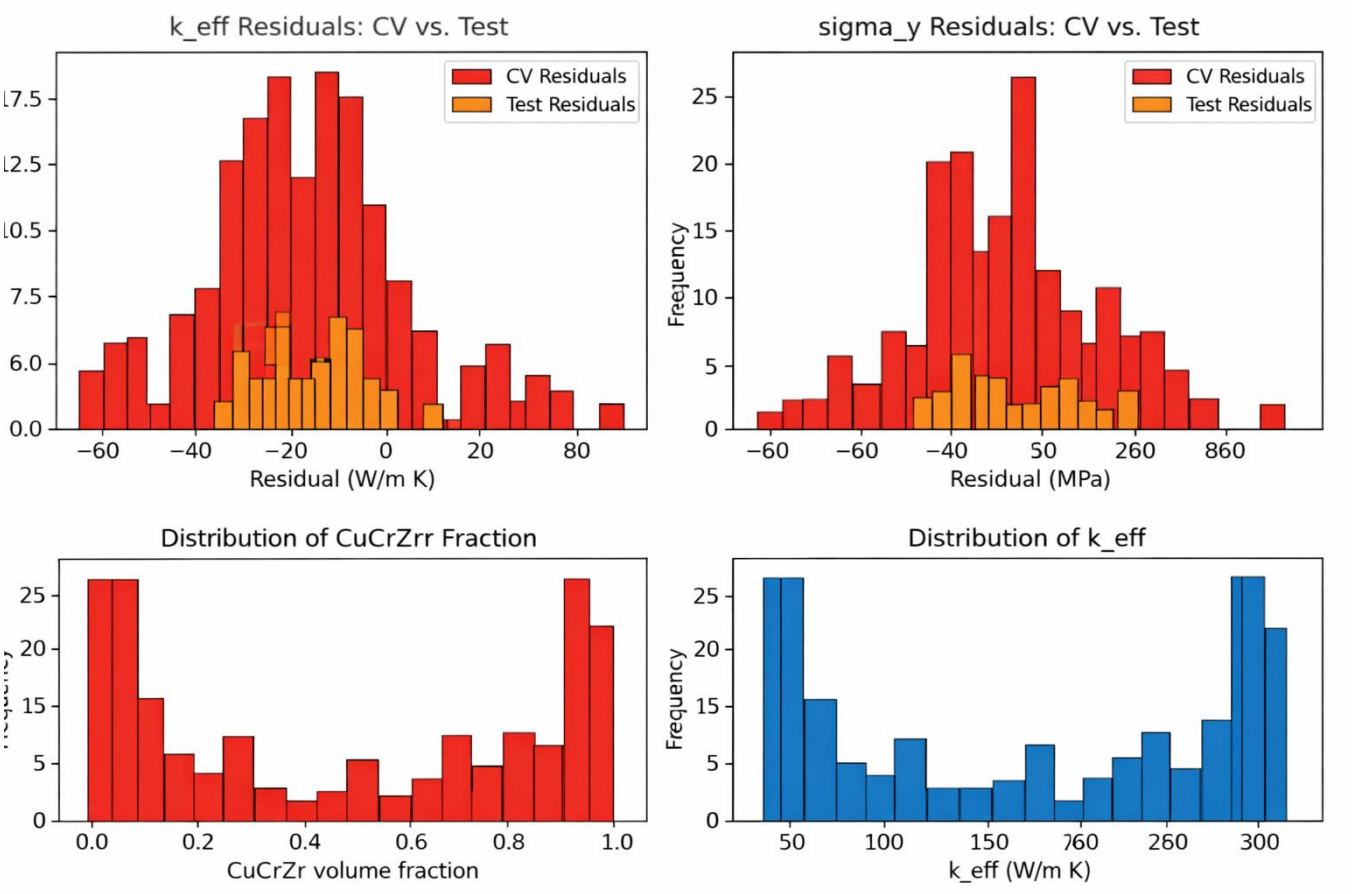

Figure 4. Prediction residuals and property distributions for the simulated graded dataset, including keffk_{eff}keff, σy\sigma_yσy , CuCrZr fraction, and effective thermal conductivity.

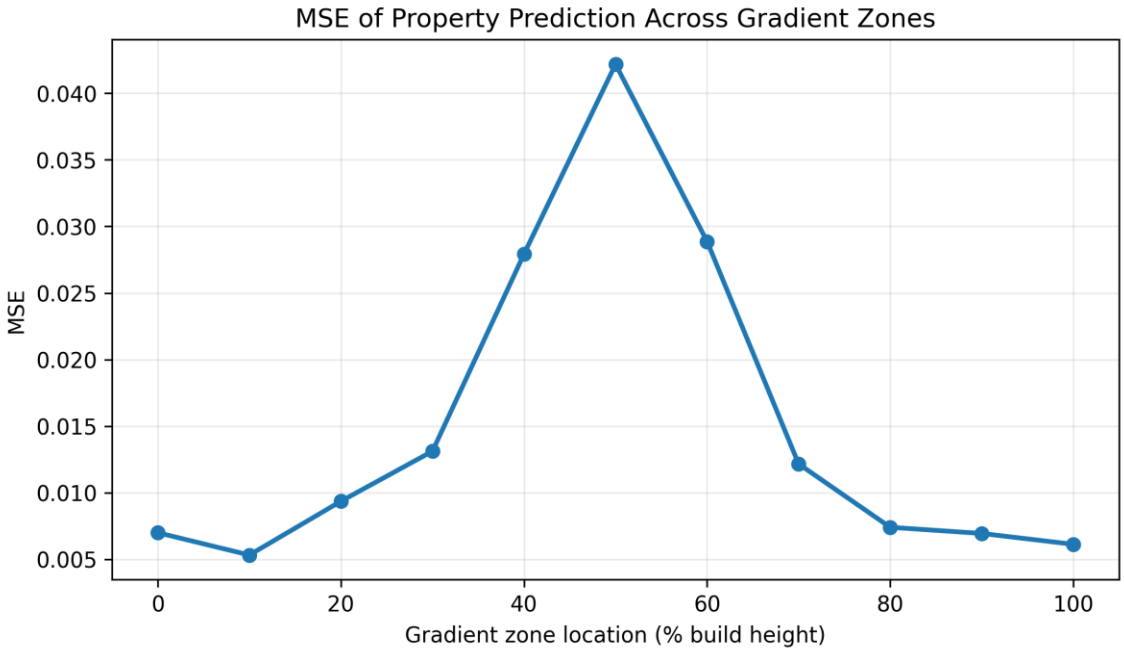

Figure 6. Mean squared error of property prediction across gradient zones, showing higher error near the composition transition region.

4.2 Engineering interpretation

The most important engineering result is that the graded architecture reduces the severity of the interface. In a discrete joint, elastic modulus, thermal conductivity, yield strength, and thermal expansion behavior change abruptly. Under thermal cycling or mechanical loading, this discontinuity can produce stress concentration and early damage accumulation. In the proposed FGM, the transition is distributed across a finite region, which lowers the local property gradient and provides a more gradual load-transfer path.

For thermal engineering components, the increase in effective conductivity is especially important. The CuCrZr-rich region provides an efficient heat-transfer path, while the 316L-rich region preserves structural support. This combination is useful for compact heat exchangers, conformal cooling inserts, thermal protection components, tooling inserts, and high-duty mechanical parts exposed to thermal gradients.

5. Conclusions

This study presented a design-oriented framework for multi-material and functionally graded additive manufacturing of next-generation mechanical and thermal engineering components. The main purpose was to show how a graded material transition can be planned and evaluated before fabrication using clear engineering calculations and performance indicators. A representative 316L stainless steel–CuCrZr graded component was used as the case study. The results show that a smooth transition between the structural 316L-rich region and the thermally conductive CuCrZr-rich region can provide a better balance between strength and heat-transfer performance than a sharp bi-material interface. Compared with the discrete baseline, the graded design reduced thermal resistance, lowered peak thermal stress, decreased interface-risk severity, and improved mass-normalized heat-transfer capability.

The most important finding is that functionally graded design is not only a material-mixing concept; it is a practical mechanical engineering strategy for controlling stress distribution, heat flow, and local property variation within one component. By avoiding abrupt property changes, the graded structure can reduce the possibility of interface-related failure and improve the reliability of parts used in thermal-management systems, tooling inserts, compact heat exchangers, aerospace brackets, and energy-system components. This study also shows that early-stage analytical modeling can help engineers compare gradient designs before manufacturing. However, the present work is based on representative numerical calculations, so experimental validation is still necessary. Future work should include fabricated 316L–CuCrZr samples, microstructural analysis, hardness mapping, tensile testing, thermal conductivity measurement, residual-stress evaluation, and finite-element simulation.

Overall, the findings suggest that multi-material and functionally graded additive manufacturing can become a valuable pathway for producing high-performance mechanical and thermal components, especially when material compatibility, gradient length, process energy, and service requirements are carefully considered together.

Funding: This research received no external funding.
Conflicts of Interest: The authors declare no conflict of interest.
Publisher's Note: All claims expressed in this article are solely those of the authors and do not necessarily represent those of their affiliated organizations, or those of the publisher, the editors and the reviewers.

References

[1] Nguyen DT, Meyers C, Yee TD, Dudukovic NA, Destino JF, Zhu C, Duoss EB, Baumann TF, Suratwala T, Smay JE, Dylla-Spears R. 3D-printed transparent glass. Advanced Materials. 2017;29(26):1701181. https://doi.org/10.1002/adma.201701181
[2] Derevianko OV, Derevianko OV, Zakiev VI, Zgalat-Lozynskyy OB. 3D printing of porous glass products using the robocasting technique. Powder Metallurgy and Metal Ceramics. 2022;60(9):546-555. https://doi.org/10.1007/s11106-022-00267-z
[3] Mader M, Hambitzer L, Schlautmann P, Jenne S, Greiner C, Hirth F, Helmer D, Kotz-Helmer F, Rapp BE. Melt-extrusion-based additive manufacturing of transparent fused silica glass. Advanced Science. 2021;8(23):2103180. https://doi.org/10.1002/advs.202103180
[4] Liu C, Qian B, Ni R, Liu X, Qiu J. 3D printing of multi-color luminescent glass. RSC Advances. 2018;8(55):31564-31567. https://doi.org/10.1039/C8RA06706F
[5] Zhang D, Xiao W, Liu C, Liu X, Ren J, Xu B, Qiu J. Highly efficient phosphor-glass composites by pressureless sintering. Nature Communications. 2020;11(1):2805. https://doi.org/10.1038/s41467-020-16649-z
[6] Wen X, Zhang B, Wang W, Ye F, Yue S, Guo H, Gao G, Zhao Y, Fang Q, Nguyen C, Zhang X, Bao J, Robinson JT, Ajayan J, Pulickel M, Lou J. 3D-printed silica with nanoscale resolution. Nature Materials. 2021;20(11):1506-1511. https://doi.org/10.1038/s41563-021-01111-2

[7] Toombs JT, Luitz M, Cook CC, Jenne S, Li CC, Rapp BE, Kotz-Helmer F, Taylor HK. Volumetric additive manufacturing of silica glass with microscale computed axial lithography. Science. 2022;376(6590):308-312. https://doi.org/10.1126/science.abm6459
[8] Mauro JC, Yue Y, Ellison AJ, Gupta PK, Allan DC. Viscosity of glass forming liquids. Proceedings of the National Academy of Sciences. 2009;106(47):19780-19784. https://doi.org/10.1073/pnas.0911705106
[9] Doremus RH. Glass: an overview. In: Concise Encyclopedia of Advanced Ceramic Materials. 1991;166-170. https://doi.org/10.1016/B978-0-08-034720-2.50052-6
[10] Corning Inc. Corning 9754 optical glass: product information and properties. 2023. https://www.corning.com/optical-materials. Accessed 12 Dec 2025.
[11] Arita R, Iijima M, Fujishiro Y, Morita S, Furukawa T, Tatami J, Maruo S. Rapid three-dimensional structuring of transparent SiO2 glass using interparticle photo-cross-linkable suspensions. Communications Materials. 2020;1(1):30. https://doi.org/10.1038/s43246-020-0029-y
[12] Moore DG, Barbera L, Masania K, Studart AR. Three-dimensional printing of multicomponent glasses using phase-separating resins. Nature Materials. 2020;19(2):212-217. https://doi.org/10.1038/s41563-019-0525-y
[13] Ouyang M, Zhang H, Li M, Zhang J, Gong Y, Huang X, Liu X, Qiu J, Yang Z, Dong G. 3D printing of luminescent glass with controlled distribution of emission colors for multi-dimensional optical anti-counterfeiting. Laser & Photonics Reviews. 2023;17(8):2300068. https://doi.org/10.1002/lpor.202300068
[14] Polsakiewicz D, Kollenberg W. Comparison of silver sources for silver/glass compounds by multi-material 3D-printing. Additional Conferences (Device Packaging, HiTEC, HiTEN, and CICMT). 2015;2015(CICMT):000305-000313. https://doi.org/10.4071/CICMT-THA31
[15] Mingareev I, Bautista N, Yadav D, Bhanderi A. Ultrafast laser deposition of powder materials on glass. Optics & Laser Technology. 2023;160:109078. https://doi.org/10.1016/j.optlastec.2022.109078
[16] Ben-Arfa BAE, Neto AS, Palamá IE, Salvado IMM, Pullar RC, Ferreira JMF. Robocasting of ceramic glass scaffolds: sol-gel glass, new horizons. Journal of the European Ceramic Society. 2019;39(4):1625-1634. https://doi.org/10.1016/j.jeurceramsoc.2018.11.019
[17] Doualle T, André J-C, Gallais L. 3D printing of silica glass through a multiphoton polymerization process. Optics Letters. 2021;46(2):364-367. https://doi.org/10.1364/OL.414848
[18] ISO/ASTM 52900:2021. Additive manufacturing: general principles - fundamentals and vocabulary. International Organization for Standardization; 2021. https://www.iso.org/standard/74514.html
[19] Klein J, Stern M, Franchin G, Kayser M, Inamura C, Dave S, Weaver JC, Houk P, Colombo P, Yang M, Oxman N. Additive manufacturing of optically transparent glass. 3D Printing and Additive Manufacturing. 2015;2(3):92-105. https://doi.org/10.1089/3dp.2015.0021
[20] Wang Y, Gawedzinski J, Pawlowski ME, Tkaczyk TS. 3D printed fiber optic faceplates by custom controlled fused deposition modeling. Optics Express. 2018;26(12):15362-15376. https://doi.org/10.1364/OE.26.015362
[21] Oropeza D, Firdosy S, Hofmann DC. Development of in-plane SS316 to M300 maraging steel gradients via directed energy deposition. Additive Manufacturing Letters. 2022;3:100078. https://doi.org/10.1016/j.addlet.2022.100078
[22] Schneck M, Horn M, Schmitt M, Seidel C, Schlick G, Reinhart G. Review on additive hybrid- and multi-material-manufacturing of metals by powder bed fusion: state of technology and development potential. Progress in Additive Manufacturing. 2021;6(4):881-894. https://doi.org/10.1007/s40964-021-00205-2
[23] Zhang W, Melcher R, Travitzky N, Bordia RK, Greil P. Three-dimensional printing of complex-shaped alumina/glass composites. Advanced Engineering Materials. 2009;11(12):1039-1043. https://doi.org/10.1002/adem.200900213
[24] Brun P-T, Inamura C, Lizardo D, Franchin G, Stern M, Houk P, Oxman N. The molten glass sewing machine. Philosophical Transactions of the Royal Society A: Mathematical, Physical and Engineering Sciences. 2017;375(2093):20160156. https://doi.org/10.1098/rsta.2016.0156
[25] Inamura C, Stern M, Lizardo D, Houk P, Oxman N. High fidelity additive manufacturing of transparent glass structures. In: Proceedings of the IASS Annual Symposia. International Association for Shell and Spatial Structures; 2018. p. 1-8.
[26] Baudet E, Ledemi Y, Larochelle P, Morency S, Messaddeq Y. 3D-printing of arsenic sulfide chalcogenide glasses. Optical Materials Express. 2019;9(5):2307-2317. https://doi.org/10.1364/OME.9.002307
[27] Zaki RM, Strutynski C, Kaser S, Bernard D, Hauss G, Faessel M, Sabatier J, Canioni L, Messaddeq Y, Danto S, Cardinal T. Direct 3D-printing of phosphate glass by fused deposition modeling. Materials & Design. 2020;194:108957. https://doi.org/10.1016/j.matdes.2020.108957
[28] Huang TS, Rahaman MN, Doiphode ND, Leu MC, Bal BS, Day DE, Liu X. Freeze extrusion fabrication of 13-93 bioactive glass scaffolds for repair and regeneration of load-bearing bones. Journal of Materials Science: Materials in Medicine. 2011;22:515-523. https://doi.org/10.1007/s10856-011-4236-4
[29] Luo J, Gilbert LJ, Qu C, Morrow B, Bristow DA, Landers RG, Goldstein J, Urbas A, Kinzel EC. Solid freeform fabrication of transparent fused quartz using a filament fed process. In: Proceedings of the 26th Annual International Solid Freeform Fabrication Symposium; 2015; Austin, TX.
[30] Fateri M, Gebhardt A. Selective laser melting of soda-lime glass powder. International Journal of Applied Ceramic Technology. 2015;12(1):53-61. https://doi.org/10.1111/ijac.12338
[31] Nan B, Gołbiewski P, Buczyński R, Galindo-Rosales FJ, Ferreira JMF. Direct ink writing glass: a preliminary step for optical application. Materials. 2020;13(7):2020. https://doi.org/10.3390/ma13071636
[32] Nazir A, Gokcekaya O, Billah KMM, Ertugrul O, Jiang J, Sun J, Hussain S. Multi-material additive manufacturing: a systematic review of design, properties, applications, challenges, and 3D printing of materials and cellular metamaterials. Materials & Design. 2023;226:111661. https://doi.org/10.1016/j.matdes.2023.111661
[33] Wu Z, Wilson-Heid AE, Griffiths RJ, Elton ES. A review on experimentally observed mechanical and microstructural characteristics of interfaces in multi-material laser powder bed fusion. Frontiers in Mechanical Engineering. 2023;9:1087021. https://doi.org/10.3389/fmech.2023.1087021
[34] Mussatto A. Research progress in multi-material laser-powder bed fusion additive manufacturing: a review of the state-of-the-art techniques for depositing multiple powders with spatial selectivity in a single layer. Results in Engineering. 2022;16:100769. https://doi.org/10.1016/j.rineng.2022.100769

[35] Chowdhury S, Yadaiah N, Prakash C, Ramakrishna S, Dixit S, Gupta LR, Buddhi D. Laser powder bed fusion: a state-of-the-art review of the technology, materials, properties and defects, and numerical modelling. Journal of Materials Research and Technology. 2022;20:2109-2172. https://doi.org/10.1016/j.jmrt.2022.07.121

[36] Schneck M, Horn M, Schmitt M, Seidel C, Schlick G, Reinhart G. Review on additive hybrid- and multi-material-manufacturing of metals by powder bed fusion: state of technology and development potential. Progress in Additive Manufacturing. 2021;6:881-894. https://doi.org/10.1007/s40964-021-00205-2

[37] Gu H, Wei C, Li L, Ryan M, Setchi R, Han Q. Numerical and experimental study of molten pool behaviour and defect formation in multi-material and functionally graded materials laser powder bed fusion. Advanced Powder Technology. 2021;32:4303-4321. https://doi.org/10.1016/j.apt.2021.09.036

[38] Mukherjee T, Zuback JS, Zhang W, DebRoy T. Residual stresses and distortion in additively manufactured compositionally graded and dissimilar joints. Computational Materials Science. 2018;143:325-337. https://doi.org/10.1016/j.commatsci.2017.11.026

[39] Rankouhi B, Islam Z, Pfefferkorn FE, Thoma DJ. Characterization of multi-material 316L-Hastelloy X fabricated via laser powder-bed fusion. Materials Science and Engineering: A. 2022;837:142749. https://doi.org/10.1016/j.msea.2022.142749

[40] Marques A, Cunha A, Gasik M, Carvalho O, Silva FS, Bartolomeu F. Inconel 718-copper parts fabricated by 3D multi-material laser powder bed fusion: a novel technological and designing approach for rocket engine. The International Journal of Advanced Manufacturing Technology. 2022;122:2113-2123. https://doi.org/10.1007/s00170-022-10011-x

[41] Mostafaei A, Zhao C, He Y, Reza Ghiaasiaan S, Shi B, Shao S, et al. Defects and anomalies in powder bed fusion metal additive manufacturing. Current Opinion in Solid State and Materials Science. 2022;26:100974. https://doi.org/10.1016/j.cossms.2021.100974

[42] Martin AA, Calta NP, Khairallah SA, Wang J, Depond PJ, Fong AY, et al. Dynamics of pore formation during laser powder bed fusion additive manufacturing. Nature Communications. 2019;10:1987. https://doi.org/10.1038/s41467-019-10009-2

[43] Luo Q, Yin L, Simpson TW, Beese AM. Effect of processing parameters on pore structures, grain features, and mechanical properties in Ti-6Al-4V by laser powder bed fusion. Additive Manufacturing. 2022;56:102915. https://doi.org/10.1016/j.addma.2022.102915